AIP Journal of Applied Physics

Aging of nano-morphology, resistivity, and far-infrared absorption in gold-black

Deep Panjwani, Aniruddha Dutta, Janardan Nath, Helge Heinrich, and Robert E. Peale

Citation: Journal of Applied Physics **118**, 154307 (2015); doi: 10.1063/1.4933178
View online: http://dx.doi.org/10.1063/1.4933178
View Table of Contents: http://scitation.aip.org/content/aip/journal/jap/118/15?ver=pdfcov
Published by the AIP Publishing

Aging of nano-morphology, resistivity, and far-infrared absorption in gold-black

Deep Panjwani, Aniruddha Dutta, Janardan Nath, Helge Heinrich, and Robert E. Peale
Department of Physics, University of Central Florida, Orlando, Florida 32816, USA

(Received 20 July 2015; accepted 2 October 2015; published online 19 October 2015)

Gold black is a highly porous, extremely fragile, infrared-absorbing film used primarily as a coating for bolometers. Long term stability of its absorbance is a significant practical concern. This paper reports on the aging of morphological, electrical, and optical properties of gold black samples prepared with different initial porosities. An observed two-fold decrease in electrical resistance after 90 days at room-temperature is correlated with an increase in nano-crystalline grain size. Much larger resistance drops were observed after isothermal annealing at temperatures up to 100 °C. Aging and annealing tended to improve the far-infrared absorption. Samples with the highest initial porosity have the fastest structural relaxation. © *2015 AIP Publishing LLC*.
[http://dx.doi.org/10.1063/1.4933178]

I. INTRODUCTION

Gold-black is a highly porous deposit produced by thermal evaporation in the presence of inert gas. Collisions with the gas molecules allow gold vapor to coalesce into nano-crystalline chains that diffuse towards the cooled substrate to form a loosely bound three-dimensional porous layer, which absorbs a broad spectrum of electromagnetic radiation.[1–3] Inert gas pressures exceeding 1 Torr result in extremely porous coatings with volume fill fractions of gold less than ~1%. The high absorption across the UV to sub-mm wavelength range is explained by macroscopic electrodynamics with an effective permittivity.[4,5] Such coatings have refractive indices n close to unity and low extinction coefficients κ to give negligible reflection at the surface, while the absorptance A is nearly unity.[6,7] (Absorptance A is the ratio of the energy absorbed to the energy incident, and it is related to transmittance T and reflectance R by energy conservation according to $A + T + R = 1$. Scattering is neglected since structural features are much smaller than IR wavelengths.)

Gold-black has found application as an absorptive coating on far-infrared bolometers for over half a century.[8,9] Extreme fragility complicates patterning for selective deposition on pixels in a detector array.[10] However, we recently developed and reported success by photolithography[11] and stencil lithography.[12] Besides macroscopic mechanical instability, microscopic stability is also a concern as it affects electrical and optical properties over time.

To study the effects of aging, we fabricated gold-black coatings with different porosities and characterized the changes in electrical resistance, thickness, and reflectance over time, both at room- and elevated- temperatures. Though gold-black films have been reported to shrink with age,[13] our observations challenge the universality of this effect, because in contrast we observe a swelling. We do observe a drop in electrical resistance over time at all temperatures, which hence seems to be a universal effect. Based on our results, resistance and thickness are uncorrelated and can change independently. Thus, the decrease in resistance with aging must have another explanation than simple macroscopic change in morphology.

We used High-Resolution Transmission Electron Microscopy (HR-TEM) to study grain boundaries and twinning defects in gold black nanoparticles, as has been done for gold nanoparticles fabricated differently.[14,15] Porous gold-black is a nanoparticle aggregate with large numbers of such boundaries and defects. Individual nano-crystallites are as small as ~2 nm, and for these we observe that room temperature thermal energy suffices to grow the grains by annealing of defects and boundaries.[16,17] The smaller the crystallite size, the more susceptible they are to growth. Similar coalescing of silver nanoparticles at room temperature when surfactants are evaporated has been reported.[18,19] These studies also reported a large drop in resistivity correlated with the coalescing process. We suggest that such room-temperature grain growth, without loss of porosity, explains the drop in electrical resistance observed over time in gold-black films. These effects are correlated with an increase in far-IR absorptance, so that aging of gold-black coatings can benefit their infrared applications.

II. EXPERIMENT

Gold-black coatings were deposited on various substrates by thermal evaporation in an evacuated bell jar back-filled with N_2. A thermoelectric cooler maintained the substrate at −13 °C. Molybdenum boats were filled with 121 mg of 99.99% pure gold. The distance between the substrate and the molybdenum boat was 10 cm. The porosity of the coating depends on the N_2 pressure during the evaporation, and the resistivity of the as-grown films increases with porosity. By using pressures inside the chamber between 0.3 and 3 Torr, we obtained coatings with sheet resistances in the range of 10^2–10^6 Ω/sq.

Film thicknesses were determined from cross-sectional micrographs of gold black coatings deposited on Si substrate, which were obtained using a Zeiss Ultra-55 Scanning Electron Microscope (SEM). Carbon tape was used to attach

the sample to a holder at 90° to the horizontal, so that the edge of the sample faces upward toward the electron gun. The uncertainty in this angle was less than 5°, so that the influence of sample orientation on the uncertainty in the measured thickness was 0.4%. For films of ~10 μm thickness, this amounts to 40 nm. This value is larger than the accuracy of the distance measurements in SEM, which is calibrated bi-annually and is observed to be stable, but it is much less than the observed thickness changes with age. The density was determined from the mass measured on a microbalance before and after the deposition, the measured thickness, and the area. Comparison to the bulk density of 19.3 g/cm^3 for gold determines the porosity. The evaporation rate in Table I was calculated from the total mass of gold in the evaporation boat and the time to evaporate all of it. In most cleaved samples, the thickness determined from the cross-section was uniform across the substrate. Some samples did show much higher thickness at the edges after cleaving due to accidental shearing during the cleave. From the pool of multiple samples imaged, we specifically chose for aging studies those which showed no sign of such alteration.

To obtain sheet resistance of the extremely fragile gold-black films by the four-probe method, four parallel gold electrodes were photo-lithographically deposited on a non-conductive plastic substrate, and the films were deposited on top of these. Since the thickness of the coating is negligible compared to the separation between the electrodes, the sheet resistance is given by[20]

$$R_S = 4.53 \times \left(\frac{V}{I}\right). \quad (1)$$

With a known applied current I (ampere) passed between the outer pair of electrodes, the voltage V (volts) was measured between the inner pair. Measured sheet resistance R_s (ohm/square) was independent of driving current for values from 0.3 to 2 mA, i.e., Joule heating effects are negligible below 2 mA. Higher currents caused sheet resistance changes due to thermal breakdown and transformation of the film. For accelerated aging studies, the four-probe substrate with the deposited film was annealed on a hot plate.

To study aging of nano-crystallites, extremely sparse gold-black was deposited over a 3 mm Cu TEM grid coated with an amorphous carbon film. The evaporation boat was loaded with just 76 μg of gold, and current was applied for just 3 s. The N_2 pressure inside the chamber during evaporation was 300 mTorr. To locate the same region for comparison after aging, the grid center was taken as reference point. Grains were imaged using a TEM TECNAI F30 operating at 300 kV and equipped with a field emission source. The electron beam current during TEM measurements was minimized pre-sample using beam deflectors to prevent local heating and annealing. The imaging integration time was maintained at 80 ms to limit annealing or damage by the electron beam. The total time a sample area was exposed to the electron beam was less than 2 s per image. The electron flux was estimated from image pixel intensities and pixel sizes.

Far-IR reflectance spectra were collected using a vacuum-bench BOMEM DA8 Fourier spectrometer equipped with Globar source, DTGS detector, and 3 or 12 μm Mylar pellicle beam-splitter, giving 22–50 μm or 50–125 μm wavelength ranges, respectively. The reflectance accessory was contained entirely within the spectrometer's evacuated sample compartment. The accessory collimates the usual focused beam within the sample compartment using a concave mirror. This collimated light is incident on the sample at 8° angle of incidence. The parallel reflected light from the sample is diverged at a proper angle using a second concave mirror, so that the beam enters the detector module at its expected acceptance angle. The gold-black was deposited on a silicon substrate coated with 200 nm thick gold on a 5 nm Cr sticking layer. An uncoated gold mirror was used as reference. Transmittance through the samples and reference was zero. The reflectance is averaged over the 10 mm diameter beam spot size on the sample surface.

For convenience in characterization, we used several different substrates, which (as noted above) were Si, gold-coated Si, plastic, and carbon-coated Cu TEM grid. A question arises as to whether the choice of substrate affects the properties of the deposited film, even when all other conditions are fixed. To our knowledge, there has been no study regarding such an effect. We reasonably suppose that the interactions between the nano-particles and the substrate, and between each other, are so weak as to make any substrate dependence improbable. However, there is one effect we have accounted for, and that is the dependence on substrate thermal conductivity, since the substrates are cooled during deposition. To allow the lower-thermal-conductivity substrates time to equilibrate, we waited 5 min after the thermoelectric cooler block reached its target temperature before initiating the evaporation.

III. RESULTS

Fig. 1 presents top-view and cross-sectional SEM images for coatings deposited on Si substrate at 0.3, 1.5, and 3.0 Torr N_2 pressure. Thickness and the size of the largest pores clearly increase with N_2 pressure. Table I presents the porosity data, which are obtained by subtracting the ratio of gold-black and bulk-gold densities from unity. Table I shows the porosity to be more than 97% in all the coatings.

TABLE I. Porosity, average sheet resistance, and resistivity of gold-black coatings deposited on Si substrate with different N_2 chamber pressures.

Coating type	N_2 pressure (Torr)	Evaporation rate (mg/s)	Porosity (%)	Sheet resistance (Ω/sq)	Resistivity (Ω m)
1	0.3	1.59	97.5	313	1.24×10^{-03}
2	1.5	0.97	98.8	1935	3.25×10^{-02}
3	3.0	1.47	99.6	32 330	8.01×10^{-01}

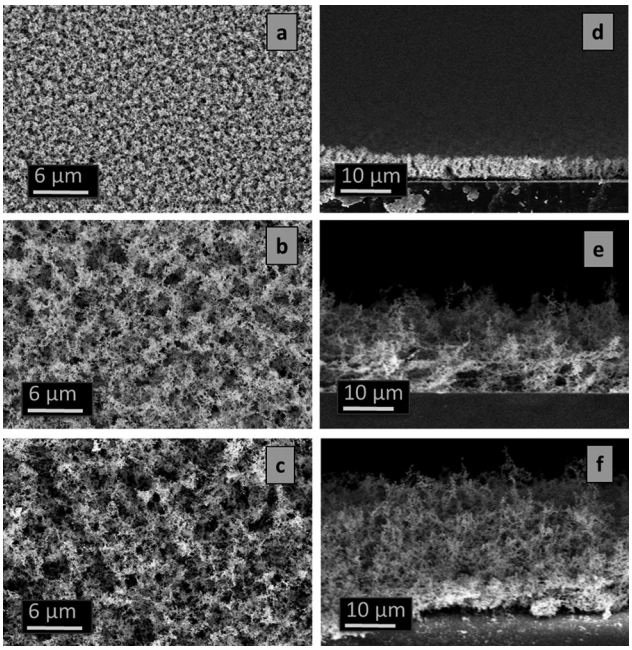

FIG. 1. SEM top-view (left) and cross-section (right) images of gold black deposited on Si substrate in N_2 pressure of 0.3 (a) and (d), 1.5 (b) and (e), and 3.0 Torr (c) and (f).

The gold-black resistivity values in Table I are 5–7 orders of magnitude higher than the value for bulk gold, which can be attributed mainly to the high porosity. However, grain boundaries scatter carriers[21–23] and also contribute to the resistivity. This effect is considered in more detail below.

Fig. 2 presents bright field TEM images, which reveal nano-crystals with grain sizes of 5–10 nm and numerous grain boundaries. Fig. 2 also reveals nano-structural changes due to aging at room temperature. The TEM electron flux was 4.13×10^5 electrons/nm^2 s for Figs. 2(a) and 2(b), while for Figs. 2(c) and 2(d) it was 3.75×10^6 electrons/nm^2 s. These fluencies are sufficiently low to avoid modifying the nano-crystalline structure. In Fig. 2(a), the grain boundaries between the loosely adjoining particles are clearly visible within the highlighted circle. Fig. 2(c) presents the same region after 90 days at room temperature, and now grain boundaries are no longer clearly distinguishable within the highlighted circle, though the aggregate structure still consists of multiple and overlapping grains. After aging, there are fewer very dark regions, indicating that the vertical stacking of overlapping grains is reduced by lateral necking between grains, which is a known behavior for coalescing particles during annealing.[24]

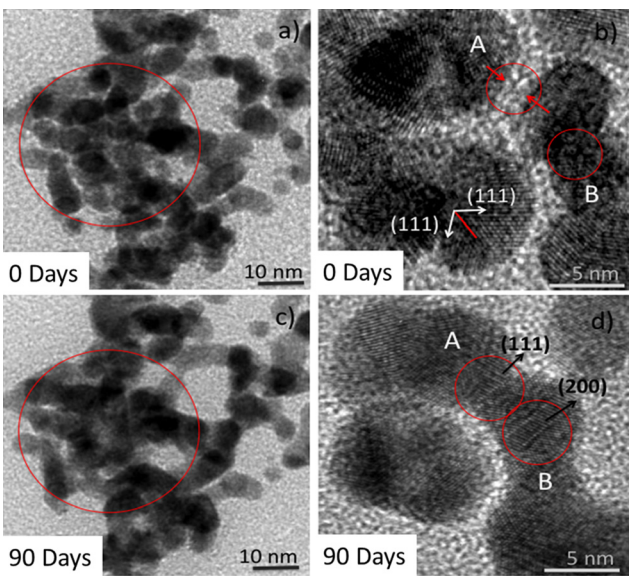

FIG. 2. TEM images of gold black features before ((a) and (b)) and after ((c) and (d)) aging of 90 days.

Fig. 2(b) shows a different region of the sample, which has a high density of twin defects, where one part of the crystal is a mirror image of the other. One example of a defect is highlighted in the image with rotated (111) planes merging at a twin boundary (red line). Fig. 2(b) also shows that the characteristic size of the single crystals is as small as ~2 nm due to these defects. Fig. 2(d) presents a TEM image of the same region after 90 days of room-temperature aging. Single crystal regions near the edges of grains A and B have moved towards each other and formed a neck, which provides an atomic diffusion path for further coalescence, the process known as aggregation.[25] In region B, after aging, twinning defects are partially removed. The dark regions, which represent overlapping of multiple grains, appear less often after aging. This is due to unification of overlapping grains, assisted by both grain rotation and surface diffusion.[26]

Fig. 3 presents the effect on sheet resistance of room-temperature aging for two separately prepared batches of films. In batch 2, the sheet resistance on three different samples was measured twice after 90 days, and the value was found to be $(55 \pm 37)\%$ of that for the as-deposited films. Seven samples measured from batch 1 after 60 days showed a sheet resistance value that was reduced to $(43 \pm 18)\%$ of the initial value.

Fig. 4 presents cross-sectional SEM images of the same region of a gold-black film before and after aging for 90 days at room temperature. Thickness of the coating was measured at 25 different locations using ImageJ in the SEM micrograph shown in Figure 4. The thickness *increased* from (16.06 ± 0.88) to $(21.24 \pm 1.02)\,\mu$m after aging. The observed increase in film thickness by 5.2 μm is significant.

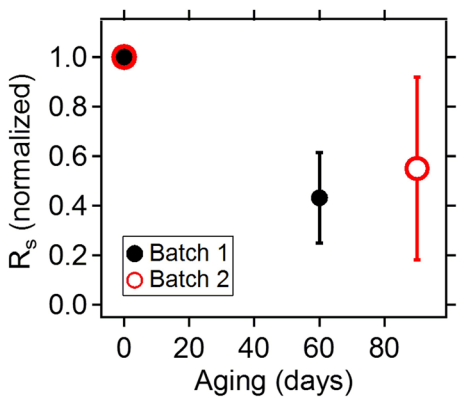

FIG. 3. Aging effect on sheet resistance at room temperature. The values are normalized to the initial value.

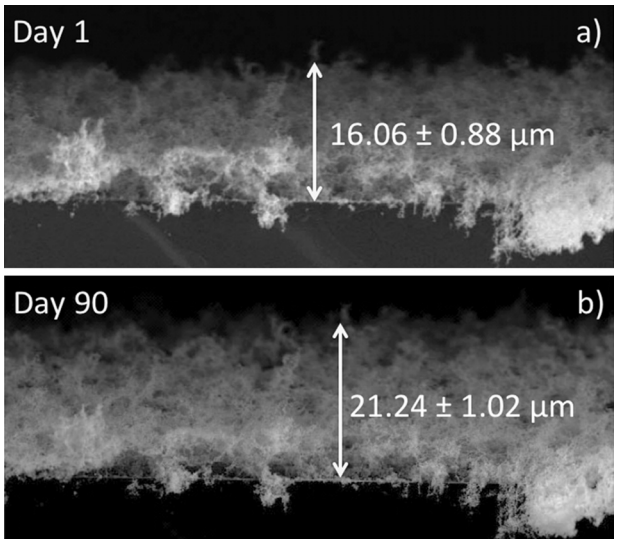

FIG. 4. Cross-section SEM image of gold-black coating before (a) and after (b) aging at room temperature for 90 days.

We tentatively suggest that the expansion is caused by the absorption of water vapor. A similar expansion was observed for three other samples, and this contrasts with the shrinkage that has been reported previously.[13]

When samples are annealed at sufficiently high temperature, they shrink rather than expand. This is obvious since the limit is a melting transition that converts gold black to a thin gold film. Figure 5 presents a plot of film thicknesses before and after aging at different temperatures for 2 h, except room temperature aging is for 90 days. Thickness for each sample is measured from SEM cross sections in more than 20 locations, and as in Fig. 4 the same locations could be located after aging based on morphological features. Aging causes an expansion at temperatures up to 70 °C, although it is statistically significant only at room temperature. Aging at 105 °C causes statistically significant shrinkage, which is associated with decrease in infrared absorption.

Fig. 6 presents the sheet resistance data vs. time for a set of isothermal anneals on type 2 and 3 coatings. The different samples were held at different constant temperatures in the range of 55–100 °C for up to 2 h. The sheet resistance shows a rapid initial drop followed by a tendency to stabilize at a

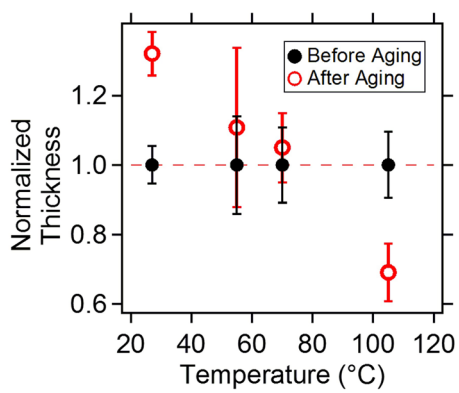

FIG. 5. Normalized thickness before and after aging at different temperatures for 2 h, except room temperature aging is for 90 days.

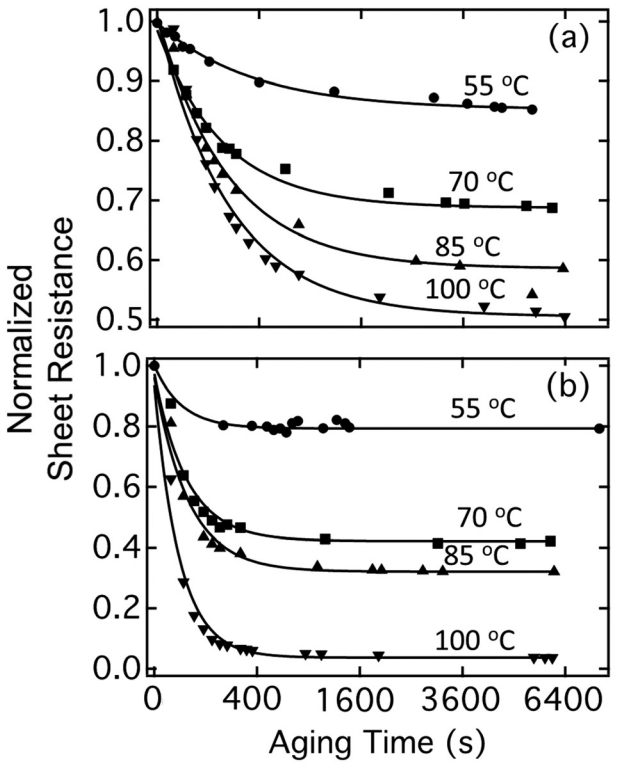

FIG. 6. Sheet resistance vs time at different temperatures for (a) type 2 and (b) type 3 gold-black coatings. (Types are defined in Table I.) Symbols are experimental data and lines are fitted curves using Eq. (2).

constant value. Resistance of type 3 coatings dropped more and stabilized sooner compared to type 2 coatings. Curves for type 1 coatings (not shown) were similar to those for type 2. The saturation of the resistance changes can be attributed to a limiting of grain growth due to pinning.[27] Once the nano-crystal reaches a certain size, it ceases to grow further at a particular temperature. Mazurin[28] describes isothermal grain growth by a structural relaxation model, which in nano-crystalline materials describes also the time-dependence of the resistivity,[29] according to which (ignoring the small change in film thickness)

$$R_s(t) - R_{s\infty} = (R_{s0} - R_{s\infty})\exp\left(-\left(\frac{t}{\tau}\right)^z\right). \qquad (2)$$

The sheet resistance terms R_{s0} and $R_{s\infty}$ are affected by grain size at times $t = 0$ and ∞, respectively, so that τ is interpreted as the grain-growth relaxation time. Measured sheet resistance values are nearly proportional to the resistivity due to the nearly constant film thickness. The exponent z is the relaxation order, which can vary from 0 to 1 with the latter holding when grain size increases linearly in time.[27] Since grain growth for nano materials such as gold black is usually non-linear in time, we adopt the usual practice of taking z to have the intermediate value 0.5.[27] In Fig. 6, the experimental data are fitted with Eq. (2), and the agreement of the lines with the data demonstrates the suitability of the model represented by Eq. (2).

Fig. 7 presents the relaxation time τ extracted from fitted curves in Fig. 6. Relaxation times tend to be longer for

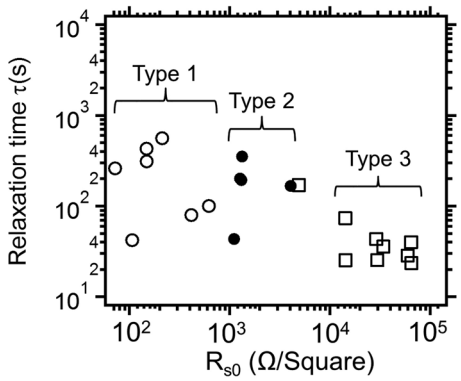

FIG. 7. Relaxation time vs. initial sheet resistance for gold-black.

coatings with lower initial sheet resistance, and the scatter in their values is higher. High porosity and high initial-resistance are consistently correlated with fast relaxation.

The reflectance spectrum for any non-magnetic material that is described by macroscopic electrodynamics can be calculated from the frequency dependent complex permittivity $\varepsilon(\omega)$. For conductors, the leading term in the expansion of $\varepsilon(\omega)$ in powers of ω is[30] the purely imaginary $i\sigma/\omega\varepsilon_0$ (in S.I. units), where σ is the DC conductivity and ε_0 is the permittivity of free space. The next term in the expansion is a real constant, which is taken to have the value unity.[7] Thus

$$\varepsilon(\omega) = 1 + i\frac{\sigma}{\omega\varepsilon_0}, \tag{3}$$

which we expect to be applicable at far-IR and lower frequencies. Fig. 8 presents the far-IR reflectance spectrum R of a type 3 sample before and after room temperature aging for 90 days. The theoretical curves are for normal-incidence reflectivity using Eq. (3) in a 3-layer (vacuum, gold-black, gold) Fresnel's equations calculation. In Eq. (3), σ was found from the measured DC sheet resistance and the fitted film thickness values d of 16 and 21 μm based on measurement in SEM cross-sections before and after aging, respectively. Aging caused the conductivity to increase from 100 to 115 S/m and the reflectivity to decrease. The experiment and theory match reasonably well, considering the simplicity of the permittivity model Eq. (3). The slow oscillation in the spectra is attributed to Fabry-Perot resonance, for which the period in wavenumbers is $1/(2\,n\,d) \sim 250\,\mathrm{cm}^{-1}$ with $n \sim 1$. The decrease in reflectance with aging is due to an increase in absorptance by up to 17%.

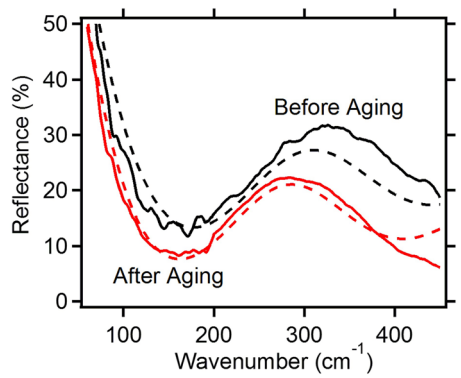

FIG. 8. Measured (solid line) and calculated (dashed line) reflectance spectra before and after room temperature aging for 90 days.

Fig. 9 presents the effect of isothermal annealing for 2 h at elevated temperatures on reflectance for samples of $\sim$10 μm thickness. The difference in the shape of the spectra compared with Fig. 8 is attributed to a film thickness that is too small for Fabry-Perot resonances to appear at such long wavelengths. (Measurements and calculations at wavelengths below 20 μm wavelength do show oscillations for these samples.) Calculated spectra based on Eq. (3) are plotted and agree with these data equally well as they did in Fig. 8. The reflectance decreased on annealing with the largest decrease occurring for the lowest annealing temperature. SEM cross sections showed that the thickness increased by 10% and 1% after a couple of hours at 55 °C and 70 °C, respectively. Thickness dropped by 11% after aging at 105 °C, and the smallest reflectance decrease occurs for this sample.

IV. DISCUSSION

The high density of defects in gold black is due to the method of fabrication. During the evaporation, the gold particles collide with N_2 gas molecules and lose energy, increasing the rate of collisions with one another. After reaching a certain grain size, they lack sufficient energy to heal defects as they coalesce. The resulting structure comprises overlapping nano-chains with many grain boundaries and twin

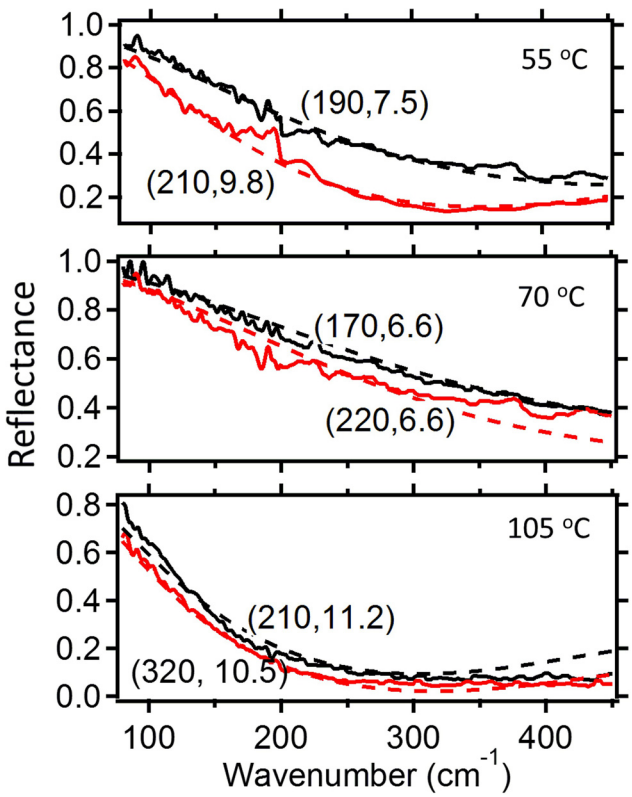

FIG. 9. Measured (solid) and calculated (dashed) reflectance spectra before (black) and after (red) accelerated aging at elevated temperatures for 2 h. Conductivities and thickness values utilized for fitting are indicated in units of S/m and μm, respectively.

defects. For FCC lattices, mismatch and mis-stacking of atoms during grain nucleation are a common reason for twinning defects on planes.[31]

Advena *et al*. reported gold-black coatings that collapsed by 50% with aging of 7 days, becoming less porous and more conductive.[13] In contrast, we found no evidence of collapse. Oppositely, there was a measurable and significant expansion by ~8%. Hence, the observed drop in sheet resistance is attributed to coalescing of particles and defect annealing at the nanometer scale, rather than micron-scale collapse as previously suggested.

As the closely spaced nano particles are heated, defects are annealed out with subsequent or concurrent aggregation of particles.[25] After the aggregation saturates, removal of defects such as twinning continues for a long time until particles eventually merge into single grains. Merging into single crystallites is the final stage, though it requires high temperatures. Pinning of grain boundaries prevents complete coalescing of grains and removal of defects, but it occurs to a sufficient extent at room temperature to measurably lower the sheet resistance without any reduction in thickness.

The higher density in type 1 and 2 samples may have resulted in more dominant aggregation, during which new grain-boundary defects are formed in the necks that join particles.[24] These new defects may contribute to the comparatively long relaxation times compared with type 3 films. The higher particle separation in the latter means less aggregation by necking, so that defect annealing within individual grains is the dominant process. This would lead to early stabilization of grain size, resulting in short relaxation times. The larger drop in sheet resistance in type 3 films suggests that without the addition of new defects at necking sites, annealing causes a larger net reduction of intrinsic lattice defects than for films of types 1 and 2.

Aging also changes the optical properties of gold-black. As for any conductor, the low frequency permittivity spectrum is determined mainly by the DC conductivity. Calculations based on Fresnel's equations confirm that the increase in conductivity that appears with aging gives a corresponding increase in absorptance. Clearly, though, there must be a limit to this effect and an optimum value of conductivity, since if the film was to be annealed all the way back to bulk gold, the absorption would reduce to ~3%.

V. SUMMARY

In summary, HR-TEM of gold–black reveals nanocrystals with sizes down to ~ 2 nm, and which are separated by grain boundaries and twinning defects. These defects anneal out and the particles coalescence over time at room temperature, which is correlated with a drop in electrical resistance without a decrease in porosity. The more porous the initial film, the faster the relaxation to a steady conductivity state, and the larger the change. Aging improves the absorptance, which suggests that for applications, gold black coatings should be aged or mildly annealed after deposition to improve and stabilize performance.

[1]L. Harris, R. T. McGinnies, and B. M. Siegel, J. Opt. Soc. Am. **38**, 582 (1948).
[2]L. Harris and J. K. Beasley, J. Opt. Soc. Am. **42**, 134 (1952).
[3]L. Harris, J. Opt. Soc. Am. **51**, 80 (1961).
[4]D. J. Bergman, Phys. Rep. **43**, 377 (1978).
[5]T. Eickhoff, P. Grosse, S. Henkel, and W. Theiss, Z. Phys. B: Condens. Matter **88**, 17 (1992).
[6]W. Becker, R. Fettig, A. Gaymann, and W. Ruppel, Phys. Status Solidi B **194**, 241 (1996).
[7]W. Becker, R. Fettig, and W. Ruppel, Infrared Phys. Technol. **40**, 431 (1999).
[8]R. A. Smith, F. E. Jones, and R. P. Chasmar, *Detection and Measurement of Infrared Radiation* (Oxford University Press, 1968).
[9]N. Nelms, G. Butcher, O. Blake, R. Cole, C. Whitford, and A. Holland, Proc. SPIE **5251**, 134 (2004).
[10]N. Nelms, J. Dowson, N. Rizvi, and T. Rohr, Appl. Opt. **45**, 6977 (2006).
[11]D. Panjwani, M. Yesiltas, J. Nath, D. Maukonen, I. Rezadad, E. M. Smith, R. Peale, C. Hirschmugl, J. Sedlmair, and R. Wehlitz, Infrared Phys. Technol. **62**, 94 (2014).
[12]D. Panjwani, M. Yesiltas, S. Singh, E. D. Barco, R. Peale, C. Hirschmugl, and J. Sedlemair, Infrared Phys. Technol. **66**, 1 (2014).
[13]D. J. Advena, V. T. Bly, and J. T. Cox, Appl. Opt. **32**, 1136 (1993).
[14]R. Ristau, R. Tiruvalam, P. Clasen, E. Gorskowski, M. Harmer, C. Kiely, I. Hussain, and M. Brust, Gold Bull. **42**, 133 (2009).
[15]A. Dutta, C. J. Clukay, D. J. Freppon, A. Bhattacharya, S. M. Kuebler, and H. Heinrch, J. Microsc. **251**, 27 (2013).
[16]H. B. Liu, J. A. Ascencio, M. Perez-Alvarez, and M. J. Yacaman, Surf. Sci. **491**, 88 (2001).
[17]M. J. Yacamán, J. A. Ascencio, H. B. Liu, and J. Gardea-Torresdey, J. Vac. Sci. Technol., B **19**, 1091 (2001).
[18]D. Wakuda, K.-S. Kim, and K. Suganuma, Scr. Mater. **59**, 649 (2008).
[19]S. Magdassi, M. Grouchko, O. Berezin, and A. Kamyshny, ACS Nano **4**, 1943 (2010).
[20]D. K. Schroder, *Semiconductor Material and Device Characterization* (John Wiley & Sons, Hoboken, New Jersey, 2006), Chap. 1, Vol. 3.
[21]J. W. C. de Vries, J. Phys. F: Met. Phys. **17**, 1945 (1987).
[22]S. M. Rossnagel and T. S. Kuan, J. Vac. Sci. Technol., B **22**, 240 (2004).
[23]T. Sun, B. Yao, A. P. Warren, K. Barmak, M. F. Toney, R. E. Peale, and K. R. Coffey, Phys. Rev. B **79**, 041402 (2009).
[24]T. H. Lim, D. McCarthy, S. C. Hendy, K. J. Stevens, S. A. Brown, and R. D. Tilley, ACS Nano **3**, 3809 (2009).
[25]B. Ingham, T. H. Lim, C. J. Dotzler, A. Henning, M. F. Toney, and R. D. Tilley, Chem. Mater. **23**, 3312 (2011).
[26]J. M. Yuk, M. Jeong, S. Y. Kim, H. K. Seo, J. Kim, and J. Y. Lee, Chem. Commun. **49**, 11479 (2013).
[27]Z. Chen, C. Shek, and J. Lai, Appl. Phys. A **80**, 703 (2005).
[28]O. V. Mazurin, J. Non-Cryst. Solids **25**, 129 (1977).
[29]J. Ederth, L. B. Kish, E. Olsson, and C. G. Granqvist, J. Appl. Phys. **91**, 1529 (2002).
[30]L. D. Landau, E. M. Lifshitz, and L. P. Pitaevskii, *Electrodynamics of Continuous Media*, 2nd ed. (Elsevier, Butterworth, Heinemann, Amsterdam, 1984), Sec. 77.
[31]N. Schell, T. Jensen, J. H. Petersen, K. P. Andreasen, J. Bøttiger, and J. Chevallier, Thin Solid Films **441**, 96 (2003).